Antichiral topological phases and protected bulk transport in dual-helix Floquet lattices

Georgios G. Pyrialakos,[1] Anestis Apostolidis,[2] Mercedeh Khajavikhan,[3]
Nikolaos V. Kantartzis,[2] and Demetrios N. Christodoulides[3]
[1]*CREOL, The College of Optics and Photonics, University of Central Florida, Orlando, Florida 32816, USA*
[2]*Aristotle University of Thessaloniki, GR-54124 Thessaloniki, Greece*
[3]*Ming Hsieh Department of Electrical and Computer Engineering, University of Southern California, Los Angeles, California 90089, USA*

(Received 8 November 2022; revised 14 April 2023; accepted 23 May 2023; published 30 May 2023)

The incorporation of driven auxiliary nodes in Floquet lattices can substantially enhance their topological nature, resulting in unique nontrivial phases. Here, we develop an alternative design approach in Floquet topology by introducing a dual-helix modulation scheme that can simultaneously support a clockwise and a counterclockwise helicity in a singular unit cell. As a result, the band structure of a dual-helix configuration can parametrically deform between a conventional phase that exhibits crossed edge states and an antichiral phase with tilted unidirectional states, showcasing for the first time an antichiral phase in Floquet topological systems. An extended family of tilted and overtilted edge states is identified and topologically characterized, revealing that integer Chern and winding numbers can successfully characterize lattices that lack global topological gaps. This results in a rich dynamic response where light wave-packets can acquire different velocities at adjacent edges, and even halt or reverse their direction into unidirectional bulk channels, preserving their topological protection. To investigate these effects, we study a dual-helix photonic lattice of evanescently coupled waveguides where a nontrivial topology can now emerge on a completely stationary configuration, departing from conventional schemes that require helical variations of the lattice sites.

DOI: 10.1103/PhysRevB.107.174313

I. INTRODUCTION

In recent years, topological theories have transformed the way physical models are viewed and classified, unveiling a host of novel wave-transport phenomena in both the classical and the quantum world [1–12]. A nontrivial topological phase is associated with the emergence of unidirectional states at the edges of insulating materials, establishing new transport pathways for electron or light currents through robust boundary channels [13–15]. These topological states offer exceptional protection from backscattering and defects and have thus been advocated for a variety of technological applications, including spintronic devices, dissipationless transistors, and energy-efficient microelectronics [16–21]. Towards this new era of topological physics, photonics has also played a pivotal role by providing accessible experimental platforms in both two and three dimensions, ranging from one-way waveguide lattices to topological metamaterials [22–29].

Typically, a nontrivial topological phase is associated with a process that can break time-reversal symmetry in a lattice, such as a magnetic field or periodic driving in Floquet configurations [30–34]. Generally, the unidirectional properties of topological edge waves are dictated by the helicity of the lattice itself. In other words, a definite propagation path can be imposed by controlling either the direction of an applied magnetic field or the rotation path of the Floquet modulation (i.e., performed either clockwise or counterclockwise). In this context, an unconventional response can be realized when a diatomic lattice incorporates opposite helicity in each sublattice, leading to the formation of antichiral edge states that do not cross at a singular momentum point but rather lie along the same tilted axis [35–37]. In photonics, antichiral lattices have been exclusively demonstrated by utilizing opposing local magnetic fields, supporting edge waves that can propagate in opposite directions at intersecting boundaries [38]. In antichiral systems, the bulk band structure remains gapless and therefore it cannot be characterized by a nontrivial topological phase; i.e., the Chern numbers of the conduction and valence bands remain zero. Nonetheless, a generalization of these design principles can facilitate the exploration of novel nontrivial phases in topological lattices, which may go beyond pure chiral or antichiral states.

An intriguing question can be raised as to whether a continuous deformation between conventional topological edge states and antichiral unidirectional states is possible in time-periodic Floquet lattices. This reveals a unique opportunity to realize topological configurations that can exhibit significantly greater flexibility in their nonreciprocal dynamics. However, such a design proposition requires a topological lattice that can support arbitrary helicity in each individual sublattice. In a photonic setting, this demands precise control of the involved magnetic fields or, in the context of Floquet topology, an opposing modulation path for waveguiding elements, a requirement that is impossible to implement in conventional platforms.

In this paper, we demonstrate that an extended class of chiral and antichiral topological states can indeed be realized in Floquet lattices based on a dual-helix chain-driven approach. To accomplish this, we depart from the conven-

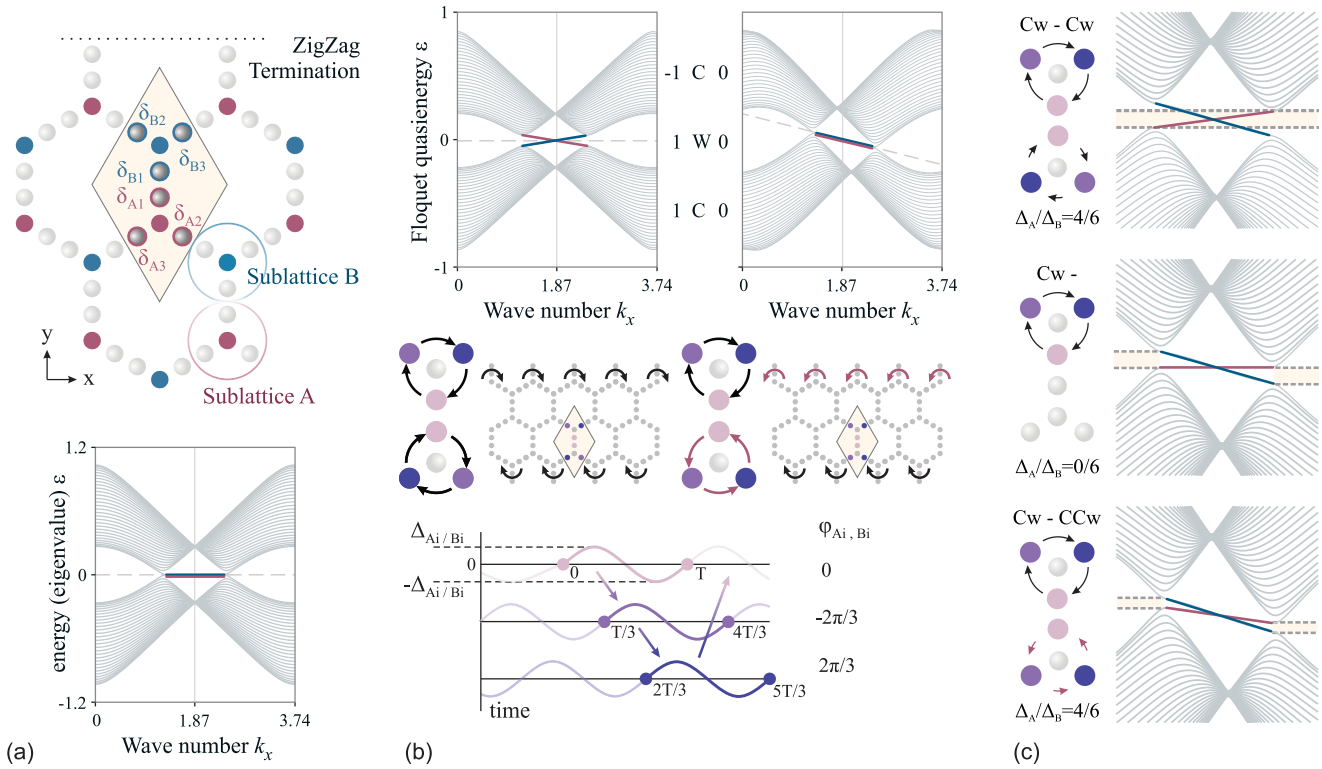

FIG. 1. (a) A honeycomb lattice can be enhanced with new degrees of freedom via the addition of six auxiliary elements, with on-site detunings $\delta_{Ai,Bi}$. A proper zigzag termination must include both auxiliary sites. The band structure is depicted near zero energy to focus on the two highlighted edge states. (b) A time-periodic modulation of $\delta_{Ai,Bi}$ is applied with a phase difference of $\phi_{Ai,Bi}$. When both sublattices acquire a clockwise helicity, the band structure becomes topologically nontrivial, encompassing a pair of crossed unidirectional edge states. When the helicity is reversed in one sublattice, the band structure becomes topologically trivial, displaying a pair of antichiral edge states. (c) For different modulation strengths or modulation phases, the band structure can continuously deform between the two limiting cases of panel (b). Here, a pair of tilted, flat and overtilted edge states are shown.

tional design approach of helical motions [see Fig. 2(a)] and instead implement a variation of bimorphic topological insulators that were recently demonstrated experimentally in photonic lattices [23]. Bimorphic configurations can manifest a nontrivial topology by employing several auxiliary elements that are modulated independently in time, preserving their position and therefore maintaining a static lattice geometry. Here, we exploit the unique strengths of bimorphic topological insulators (TIs), and in contrast to their original conception where modulation is uniform, we introduce higher complexity through several additional auxiliary nodes in the unit cell. This allows us to employ arbitrary helicity on each sublattice, showcasing an antichiral phase in Floquet topological systems. In this respect, we demonstrate that dual-helix configurations can support a continuous class of nontrivial topological edge states that may gradually deform into antichiral states by altering the modulation profile of the lattice, leading into a gapless overtiled regime characterized by integer Chern and winding numbers. In contrast to conventional topological phases, we show that the corresponding topological invariants can be determined through a k-space transformation that allows them to conform to the gapless nature of overtilted Floquet spectra.

To investigate the effects associated with antichiral Floquet systems, we examine a diverse array of boundary configurations on a dual-helix photonic waveguide lattice and demonstrate an unprecedented level of control over the transport properties of topological waves. In particular, we showcase that, in a uniform lattice geometry, one can simultaneously excite multiple unidirectional wave-packets that can propagate with arbitrary transport speeds and even opposite directions, while maintaining robust topological protection. Moreover, we reveal the presence of unidirectional bulk channels that can provide a coupling path between antichiral states residing at opposite edges, thus creating alternative means of topological protection that can involve bulk dynamics. In this regard, while bimorphic photonic TIs have made an essential step in the evolution of topological waveguide platforms by eliminating bending losses, the versatility of dual-helix configurations can further improve upon these core design principles, expanding the means to manipulate light wavepackets, towards a new generation of topological photonic circuitry.

II. THEORETICAL FRAMEWORK

To begin with, we consider a tight-binding lattice using a straightforward extension of the chain-driven design utilized by bimorphic TIs. This generalized model will be later applied to a photonic array of evanescently coupled waveguides. In this section we study a honeycomb arrangement; however, the

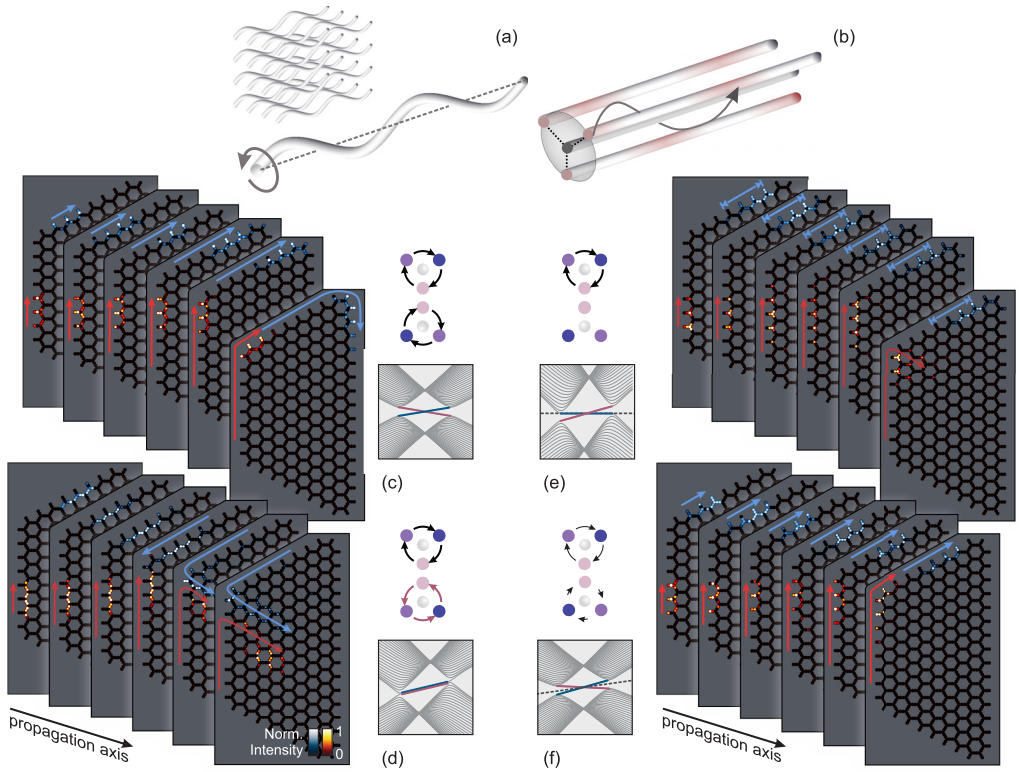

FIG. 2. (a) In a photonic waveguide array, a nontrivial topology is conventionally generated via a global helical motion of the elements along the propagation axis. Each element must follow an identical rotation path to maintain consistent couplings along z. (b) A building block of a bimorphic (chain-driven) lattice where each site is surrounded by a number of auxiliary elements. A nontrivial topology can be generated via a modulation of the effective local potentials of the three auxiliary elements (corresponding to an index variation Δn along the z axis in the context of photonic waveguides), maintaining the local position of the elements. Due to this property, two different chain-driven sublattices that exhibit a different phase, magnitude, or period in their respective auxiliary-site modulations can coexist within a singular unit cell. (c) A trapezoid configuration combines both an A and a B sublattice termination at the top edge and the left edge, respectively. Two crossed topological edges states travel unidirectionally around the lattice, wrapping around corners with zero scattering or diffraction. (d) Two antichiral edge states propagate in opposite directions, meeting at the top-left corner where they subsequently scatter into the bulk. (e, f) Reducing the modulation amplitude in one sublattice can lead to asymmetric edge state pairs. In panel (e) a wave packet remains stationary at the top edge for $\Delta_{Ai} = 0$, while in panel (f) a wave packet slows down after it crosses the top-left corner.

core principles outlined herein are universal, with a square lattice case also covered in the Supplemental Material [39].

To employ our double-helix approach we introduce two auxiliary elements for each connecting path between the primary sites of the honeycomb lattice, as depicted in Fig. 1(a). The tight-binding Hamiltonian is given by

$$H(\boldsymbol{k}) = \sum_{i=1}^{3} \delta_{Ai}(t) c_{Ai}^{\dagger} c_{Ai} + \sum_{i=1}^{3} \delta_{Bi}(t) c_{Bi}^{\dagger} c_{Bi} + H_{\kappa}(\boldsymbol{k}), \qquad (1)$$

where $\delta_{Ai}(t)$ and $\delta_{Bi}(t)$ are the on-site detunings of the six auxiliary elements and $H_{\kappa}(\boldsymbol{k})$ is the coupling Hamiltonian involving all nearest-neighbor terms. Without loss of generality, $H_{\kappa}(\boldsymbol{k})$ comprises identical couplings which are all normalized to unity. Nonetheless, one may also consider unequal couplings as long as the two sublattices remain balanced, a symmetry that protects against trivial band-gap openings. By introducing the three auxiliary chains the primitive unit cell of the honeycomb lattice is enlarged but its morphology remains identical to the diatomic variation. In this respect, due to the symmetry rules of the honeycomb lattice the static band structure displays a pair of Dirac cones that can generate two trivial edge states for a zigzag termination [Fig. 1(a)]. To avoid the formation of defect (Tamm-like) edge states the outer auxiliary chains must also be included at the terminated edge, as shown in the upper panel of Fig. 1(a). The band diagrams of Fig. 1 focus on the modes around $\beta = 0$, with the full spectra shown in the Supplemental Material [39].

Before discussing the generalized model, we begin by introducing a conventional topological phase in the dual-helix design. To do so, we implement a z-periodic modulation of the refractive indices in the six auxiliary sites, associated with the on-site detunings δ_{Ai} and δ_{Bi}, as shown in Fig. 1(b) (left). In this example, the on-site detunings follow a sinusoidal variation with a $2\pi/3$ phase shift between the three elements, $\delta_{Ai,Bi} = \Delta_{Ai,Bi} \sin(2\pi t/T + \phi_{Ai,Bi})$ and a period of $T = 7$. In this respect, when a clockwise modulation is imposed in both sublattices, with an equal amplitude on all six auxiliary sites ($\Delta_{Ai,Bi} = 6$), the Dirac gap opens and a topological pair of unidirectional edge states emerges [Fig. 1(b), left]. The lattice topological invariants, namely, the two bulk Chern numbers (C) and the Floquet winding number (W), acquire nonzero values, indicating indeed the presence of a nontrivial topological phase [39].

In order to step beyond the conventional topological phase characterized by a crossed pair of edge states, we must break the uniformity of the two sublattices. In this respect, the flexibility of the dual-helix design becomes immediately apparent. The two main sites [highlighted with red and blue in Fig. 1(a)] are surrounded by three individual neighbors which can be modulated independently from each other. In this respect, a different helicity can be imposed locally on each sublattice by a proper phase shift of the $\delta_{Ai,Bi}$ coefficients. First, we focus on the special case where the two sublattices acquire opposite helicity with equal modulation amplitudes between Δ_{Ai} and Δ_{Bi}. In this second example, the modulation phases ϕ_{A2} and ϕ_{A3} are swapped, reversing the helicity in sublattice A. The band structure associated with this design [as shown in Fig. 1(b), right], is gapless, similar to the nonmodulated case of Fig. 1(a). However, the two edge states are now noticeably tilted. This result corresponds to an explicit manifestation of a Floquet antichiral phase. A numerical characterization of the topological invariants reveals a strictly trivial phase with zero Chern numbers, as expected for antichiral edge states. Interestingly, as both edge states acquire a negative group velocity, the bottom and top zigzag edges support only a leftwise transport direction, as opposed to conventional crossed topological states which support opposite transport directions. This property has significant implications in the transport dynamics of fully finite configurations, as discussed in the following section.

Having introduced the concept of Floquet antichiral states, we now aim to generalize these results revealing the full versatility of dual-helix designs. In this respect, one can show that the two cases of Fig. 1(b) correspond to the limits of a continuous family of edge modes that can transition between conventional topological states and antichiral states. This expanded class of topological band structures is readily supported by the dual-helix approach via an autonomous variation of the Δ_{Ai} and Δ_{Bi} amplitudes. To illustrate this, we investigate the chain-driven lattice, starting from the nontrivial topological phase with a dual-helix clockwise modulation and $\Delta_{Ai,Bi} = \Delta$. In Fig. 1(c) we depict three special cases. First, the ratio Δ_{Ai}/Δ_{Bi} is decreased by lowering the modulation amplitude Δ_{Ai} of the three elements surrounding site A. The two edge states obtain a noticeable tilt while the spectrum becomes asymmetric around the crossing point. By lowering Δ_{Ai} even further we reach a critical value ($\Delta_{Ai} = 0$) where the global gap between the two photonic bands vanishes. In this case, the edge state highlighted with red obtains a vanishing group velocity and becomes flat. From this point on, by increasing the modulation with a counterclockwise helicity we are able to overtilt the two edge states, equipping both with a negative group velocity, eventually reaching the limiting case of antichiral states. It is worth noting that a similar transformation can be achieved via a multitude of means. For example, one may also consider a variation of the modulation phases instead of the amplitudes, starting with $\phi_{A1} = 0$ and $\phi_{A2} = -\phi_{A3} = \phi_A = -2\pi/3$ while keeping $\Delta_{Ai,Bi}$ and ϕ_{Bi} constant. In this respect, the complete family of topological tilted and overtilted states can be obtained within the range $\phi_A = [-2\pi/3, 2\pi/3]$.

The topological classification of this new family of tilted edge states can be properly performed by characterizing the corresponding topological invariants [13,40–44]. As shown here, the two limiting cases of Fig. 1(b) correspond to a nontrivial (left) and a trivial (right) topological phase. For the examples presented in Fig. 1(c) we first attempt an evaluation of the Chern numbers by numerically integrating the Berry curvature over the bulk Brillouin zone. We find that in all cases the Chern numbers are nontrivial ($C = -1$ and $C = 1$ for the top and bottom bands, respectively), irrespective of the presence or absence of a global gab. Consequently, this class of Floquet systems maintains a nontrivial topology, even in the overtilted gapless regime [bottom panel of Fig. 1(c)].

An additional invariant quantity in the Floquet system that can explicitly indicate the number of edge states that lie within topological gaps is the winding number W. A conventional approach to calculate W for a specific gap requires a shift of its eigenvalue to the Floquet zone boundary (at $\beta = \pi/T$) before integrating the unitary operator U over the $\boldsymbol{k}$-t space [39]. For gapped tilted cases this is a straightforward process that here yields a nontrivial integer value of $W = 1$. However, for overtilted band structures there is no universal eigenvalue β that can be associated with a global gap and a new strategy must be introduced. To overcome this issue, we propose an alternative strategy. In this respect, we choose a k-dependent branch cut for the logarithm in the effective Hamiltonian $H_{\text{eff}} = 1/T \log U(\boldsymbol{k}, T)$ and integrate over a β-$\boldsymbol{k}$ manifold that cuts through the local Dirac band gaps. By doing so, the winding number W can be successfully evaluated, revealing again a nontrivial integer value of $W = 1$ for all overtilted cases, until the limiting case of antichiral states is reached.

III. WAVE-PACKET DYNAMICS IN A PHOTONIC ARRAY

The chain-driven design principles can be applied to any configuration that allows a periodic variation of its on-site potentials. In this respect, photonic waveguide arrays provide an efficient platform to implement dual-helix topological lattices. To demonstrate this, we numerically solve the Floquet eigenvalue problem of the continuous Schrödinger equation associated with a z-periodic chain-driven lattice in a photonic waveguide array, as shown in the Supplemental Material [39]. Each waveguide is shaped as a super-Gaussian local potential with an appropriate magnitude and separation between its neighboring sites, so as to closely approximate the dynamics of the theoretical tight-binding Hamiltonian. All parameters lie well within their experimental limits. The results are in excellent agreement with the coupling model band diagrams, affirming that the classes of antichiral tilted and overtilted topological edge states can manifest themselves in a realistic photonic structure. In this section, we utilize this waveguide array to observe light-packet evolution in several dual-helix designs. The lattices are designed using an optimized set of modulation phases rather than the ones used in Fig. 1, as outlined in the Supplemental Material, Sec. 1 [39].

The transport dynamics of dual-helix chain-driven lattices are investigated via beam propagation method (BPM) simulations by employing a finite trapezoid configuration that combines both an A and a B sublattice termination at intersecting boundaries (Fig. 2). The two boundaries meet at a 120° angle in the top-left corner, acting as a "top" and a "bottom" edge of a ribbon-

like configuration, respectively. Starting with Fig. 2(c), we depict a case where both sublattices acquire the same (clockwise) helicity, displaying a conventional topological phase that encompasses a pair of crossed unidirectional edge states [corresponding to the case of Fig. 1(b), left]. The lattice is excited simultaneously at the two edges with two separate wave-packets, indicated by the red and blue intensity profiles. As expected, the two wave-packets travel unidirectionally along the boundaries, facing a clockwise direction, and eventually wrap around the corners with zero scattering into the bulk. In essence, each of the two wave-packets is paired to a clockwise topological mode and the red-to-blue arrow in the final panel corresponds to a singular transport path, due to maximal coupling between the red and the blue states.

When we impose an opposite helicity in the two sublattices (with equal modulation amplitudes) the band diagram displays a pair of antichiral edge states [corresponding to the case of Fig. 1(b), right]. In this scenario, illustrated in Fig. 2(d), the two wave-packets propagate in opposite directions, towards the upper-left corner of the lattice. Eventually, due to a mismatch of the transport directions supported by each boundary, the two wave-packets are unable to couple into the adjacent edge and instead penetrate the lattice, seemingly scattering into the bulk. At first, this appears as a failure of topological protection, a property which dictates that wave packets are immune to bulk scattering from corners or defects. However, as we see in the final example, this is far from the truth, not only for antichiral states but also for all overtilted cases.

Before further investigating the bulk scattering of overtilted states, we focus on two special cases, one lattice variation where the amplitudes Δ_{Ai} are nullified ($\Delta_{Ai} = 0$) and one case with decreased modulation amplitudes ($\Delta_{Ai} < \Delta_{Bi}$). In general, a decreased modulation amplitude allows the design of topological lattices that can support multiple transport speeds for singular wave-packets at intersecting boundaries. This feature is exclusive to dual-helix lattices due to the fact that multiple helicities can now coexist within a singular unit cell. In conventional topological lattices, one may naively attempt a similar dynamic effect by combining two individual unit cells with different helicities. However, this will fail as it will inadvertently lead to the formation of secondary topological boundaries.

In the first case, presented in Fig. 2(e), the group velocity of the blue edge state vanishes and, consequently, the blue-highlighted wave packet remains trapped in the excited waveguides, allowing only a small degree of micromotion. On the other boundary, the red edge state acquires a nonzero group velocity and the red-highlighted wave packet propagates as a conventional topological state, exhibiting unidirectional propagation at the edge. In the second case, presented in Fig. 2(f), the launched wave-packets travel unidirectionally, in a fashion similar to that of the result of Fig. 2(c), but at a different pace when traversing each edge. When meeting the top-left corner, the red wave-packet is able to fully couple to the blue-highlighted state with no scattering into the bulk, despite the mismatch in transport speeds between the red and the blue states. This example, therefore, exhibits an exclusive topological response where wave packets can traverse the boundaries of a photonic lattice with enhanced degrees of freedom.

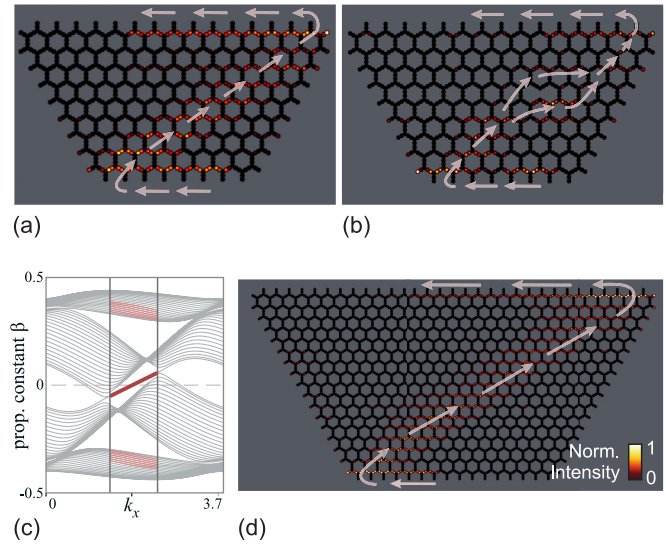

FIG. 3. (a) An antichiral state couples perfectly to unidirectional bulk modes [red-highlighted states in panel (c)] that originate from the flat band of the undriven spectrum. These bulk states create a protected channel that links two antichiral states at opposite edges. (b) Adding a defect along the path of the bulk channel causes light to travel around the missing element, revealing a new aspect of topologically protected transport. (c) The spectrum around $\beta = 0$, including the emerging unidirectional CLS. (d) A similar effect is observed in a larger lattice with roughly four times the number of elements.

To investigate the bulk scattering of overtilted topological states, in Fig. 3(a) we repeat the simulation of Fig. 2(d) by observing the red-highlighted wave packet for a longer time span, after allowing itself to scatter at the corner. Here, the field snapshots at different observations times are combined on the same panel, with their approximate positions indicated by individual arrows. In contrast to what initially appears as random diffusion of power into the bulk, the wave packet instead follows a localized unidirectional path through the lattice. After meeting the opposite edge, it couples almost fully to an antichiral edge state, continuing its path along the left boundary. This unique behavior is supported by the presence of compact localized states (CLS) that originate from the flat band of the undriven spectrum (as seen in Fig. S1 [39]). In contrast to other bulk modes, these states have the same dimensionality as edge states and are thus highly favored when mode coupling occurs due to scattering. Their group velocity [Fig. 2(c)] is almost linear and has a sign opposite that of the corresponding antichiral edge states. Thus, light can propagate across the diagonal of the lattice almost undispersed, creating a link between antichiral states at opposite edges. While in practice a small amount of power is expected to leak into the bulk (depending also on the distance between the boundaries), in the example of Fig. 2(e) approximately 95% of power is robustly transferred between the two edges.

The result of Fig. 3(a) reveals an alternative aspect of topological protection encountered exclusively in dual-helix Floquet lattices. To support this claim, we perform an additional set of simulations in a dual-helix system with a lattice defect, by removing one site directly on the path of the bulk

channel [shown in Fig. 3(b)]. The wave packet travels around the defect and an effect similar to that in Fig. 3(a) is observed. Moreover, to quantify the coupling efficiency between the two edges and the losses due to dispersion or bulk mode scattering, we repeat the simulation (without the defect) on a larger lattice. The result of Fig. 3(a) verifies that the observed effect is indeed highly robust.

IV. CONCLUSION

In conclusion, we have investigated an alternative class of dual-helix modulation schemes in Floquet lattices that can exhibit a continuous family of nontrivial topological phases with tilted, flat, and overtilted unidirectional edge states. Overtilted edge states in dual-helix Floquet systems are topologically protected and can propagate unidirectionally along the edges, while the straightforward design rules of chain-driven lattices provide increased versatility in manipulating their transport properties. In this article, we have investigated only a subset of the possible variations of dual-helix lattices, exclusively in diatomic designs. One may consider more advanced designs by freely manipulating the magnitude and the phase of each individual element or even involve unit cells with more than two sublattices, incorporating multiple local helicities. In this respect, dual-helix lattices may enable the design of advanced topological circuits that can exhibit a large variety of transport characteristics. The proposed designs can be readily implemented in photonic waveguide lattices or other similar photonic platforms that can support modulation of the on-site potentials without having to periodically shift the node positions or apply external magnetic fields.

ACKNOWLEDGMENTS

This work was partially supported by ONR MURI (Grant No. N00014-20-1-2789), AFOSR MURI (Grants No. FA9550-20-1-0322 and No. FA9550-21-1-0202), the National Science Foundation (Grants No. DMR-1420620 and No. EECS-1711230), the MPS Simons Collaboration (Simons Grant No. 733682), the W. M. Keck Foundation, the US-Israel Binational Science Foundation (Grant No. 2016381), and the US Air Force Research Laboratory (Grant No. FA86511820019). G.G.P acknowledges the support of the Bodossaki Foundation.

[1] A. B. Khanikaev, S. H. Mousavi, W.-K. Tse, M. Kargarian, A. H. MacDonald, and G. Shvets, Photonic topological insulators, Nat. Mater. **12**, 233 (2013).

[2] J. W. McIver, B. Schulte, F.-U. Stein, T. Matsuyama, G. Jotzu, G. Meier, and A. Cavalleri, Light-induced anomalous Hall effect in graphene, Nat. Phys. **16**, 38 (2020).

[3] R. Fleury, A. B. Khanikaev, and A. Alù, Floquet topological insulators for sound, Nat. Commun. **7**, 11744 (2016).

[4] M. C. Rechtsman, J. M. Zeuner, Y. Plotnik, Y. Lumer, D. Podolsky, F. Dreisow, S. Nolte, M. Segev, and A. Szameit, Photonic Floquet topological insulators, Nature (London) **496**, 196 (2013).

[5] F. Nathan, D. Abanin, E. Berg, N. H. Lindner, and M. S. Rudner, Anomalous Floquet insulators, Phys. Rev. B **99**, 195133 (2019).

[6] S. H. Mousavi, A. B. Khanikaev, and Z. Wang, Topologically protected elastic waves in phononic metamaterials, Nat. Commun. **6**, 8682 (2015).

[7] X. Cheng, C. Jouvaud, X. Ni, S. H. Mousavi, A. Z. Genack, and A. B. Khanikaev, Robust reconfigurable electromagnetic pathways within a photonic topological insulator, Nat. Mater. **15**, 542 (2016).

[8] N. R. Cooper, J. Dalibard, and I. B. Spielman, Topological bands for ultracold atoms, Rev. Mod. Phys. **91**, 015005 (2019).

[9] K. Wintersperger, C. Braun, F. N. Ünal, A. Eckardt, M. D. Liberto, N. Goldman, I. Bloch, and M. Aidelsburger, Realization of an anomalous Floquet topological system with ultracold atoms, Nat. Phys. **16**, 1058 (2020).

[10] F. N. Ünal, A. Eckardt, and R.-J. Slager, Hopf characterization of two-dimensional Floquet topological insulators, Phys. Rev. Res. **1**, 022003(R) (2019).

[11] T. Schuster, S. Gazit, J. E. Moore, and N. Y. Yao, Floquet Hopf Insulators, Phys. Rev. Lett. **123**, 266803 (2019).

[12] E. Lustig, S. Weimann, Y. Plotnik, Y. Lumer, M. A. Bandres, A. Szameit, and M. Segev, Photonic topological insulator in synthetic dimensions, Nature (London) **567**, 356 (2019).

[13] M. S. Rudner, N. H. Lindner, E. Berg, and M. Levin, Anomalous Edge States and the Bulk-Edge Correspondence for Periodically Driven Two-Dimensional Systems, Phys. Rev. X **3**, 031005 (2013).

[14] M. Hafezi, S. Mittal, J. Fan, A. Migdall, and J. M. Taylor, Imaging topological edge states in silicon photonics, Nat. Photonics **7**, 1001 (2013).

[15] M. A. Bandres, S. Wittek, G. Harari, M. Parto, J. Ren, M. Segev, D. N. Christodoulides, and M. Khajavikhan, Topological insulator laser: Experiments, Science **359**, eaar4005 (2018).

[16] J. E. Moore, The birth of topological insulators, Nature (London) **464**, 194 (2010).

[17] Q. L. He, T. L. Hughes, N. P. Armitage, Y. Tokura, and K. L. Wang, Topological spintronics and magnetoelectronics, Nat. Mater. **21**, 15 (2022).

[18] Y. Tokura, K. Yasuda, and A. Tsukazaki, Magnetic topological insulators, Nat. Rev. Phys. **1**, 126 (2019).

[19] W. G. Vandenberghe and M. V. Fischetti, Imperfect two-dimensional topological insulator field-effect transistors, Nat. Commun. **8**, 14184 (2017).

[20] L. Lu, J. D. Joannopoulos, and M. Soljačić, Topological photonics, Nat. Photonics **8**, 821 (2014).

[21] B.-Y. Xie, H.-F. Wang, X.-Y. Zhu, M.-H. Lu, Z. D. Wang, and Y.-F. Chen, Photonics meets topology, Opt. Express **26**, 24531 (2018).

[22] A. B. Khanikaev and G. Shvets, Two-dimensional topological photonics, Nat. Photonics **11**, 763 (2017).

[23] G. G. Pyrialakos, J. Beck, M. Heinrich, L. J. Maczewsky, N. V. Kantartzis, M. Khajavikhan, A. Szameit, and D. N. Christodoulides, Bimorphic Floquet topological insulators, Nat. Mater. **21**, 634 (2022).

[24] L. J. Maczewsky, J. M. Zeuner, S. Nolte, and A. Szameit, Observation of photonic anomalous Floquet topological insulators, Nat. Commun. **8**, 13756 (2017).
[25] Y. G. N. Liu, P. S. Jung, M. Parto, D. N. Christodoulides, and M. Khajavikhan, Gain-induced topological response via tailored long-range interactions, Nat. Phys. **17**, 704 (2021).
[26] S. Mukherjee, A. Spracklen, M. Valiente, E. Andersson, P. Öhberg, N. Goldman, and R. R. Thomson, Experimental observation of anomalous topological edge modes in a slowly driven photonic lattice, Nat. Commun. **8**, 13918 (2017).
[27] S. Weimann, M. Kremer, Y. Plotnik, Y. Lumer, S. Nolte, K. G. Makris, M. Segev, M. C. Rechtsman, and A. Szameit, Topologically protected bound states in photonic parity–time-symmetric crystals, Nat. Mater. **16**, 433 (2017).
[28] J. M. Zeuner, M. C. Rechtsman, Y. Plotnik, Y. Lumer, S. Nolte, M. S. Rudner, M. Segev, and A. Szameit, Observation of a Topological Transition in the Bulk of a Non-Hermitian System, Phys. Rev. Lett. **115**, 040402 (2015).
[29] S. Stützer, Y. Plotnik, Y. Lumer, P. Titum, N. H. Lindner, M. Segev, M. C. Rechtsman, and A. Szameit, Photonic topological anderson insulators, Nature (London) **560**, 461 (2018).
[30] G. Liu, N. Hao, S.-L. Zhu, and W. M. Liu, Topological superfluid transition induced by a periodically driven optical lattice, Phys. Rev. A **86**, 013639 (2012).
[31] R. Roy and F. Harper, Periodic table for Floquet topological insulators, Phys. Rev. B **96**, 155118 (2017).
[32] M. Aidelsburger, M. Atala, S. Nascimbène, S. Trotzky, Y.-A. Chen, and I. Bloch, Experimental Realization of Strong Effective Magnetic Fields in an Optical Lattice, Phys. Rev. Lett. **107**, 255301 (2011).
[33] J. Lu, L. He, Z. Addison, E. J. Mele, and B. Zhen, Floquet Topological Phases in One-Dimensional Nonlinear Photonic Crystals, Phys. Rev. Lett. **126**, 113901 (2021).
[34] B. Wang, J. Quan, J. Han, X. Shen, H. Wu, and Y. Pan, Observation of photonic topological Floquet time crystals, Laser Photonics Rev. **16**, 2100469 (2022).
[35] X. Cheng, J. Chen, L. Zhang, L. Xiao, and S. Jia, Antichiral edge states and hinge states based on the Haldane model, Phys. Rev. B **104**, L081401 (2021).
[36] E. Colomés and M. Franz, Antichiral Edge States in a Modified Haldane Nanoribbon, Phys. Rev. Lett. **120**, 086603 (2018).
[37] J. Chen, W. Liang, and Z.-Y. Li, Antichiral one-way edge states in a gyromagnetic photonic crystal, Phys. Rev. B **101**, 214102 (2020).
[38] P. Zhou, G.-G. Liu, Y. Yang, Y.-H. Hu, S. Ma, H. Xue, Q. Wang, L. Deng, and B. Zhang, Observation of Photonic Antichiral Edge States, Phys. Rev. Lett. **125**, 263603 (2020).
[39] See Supplemental Material at http://link.aps.org/supplemental/10.1103/PhysRevB.107.174313 for a further theoretical discussion and results on tilted and over-tilted topological phases.
[40] T. Kitagawa, E. Berg, M. Rudner, and E. Demler, Topological characterization of periodically driven quantum systems, Phys. Rev. B **82**, 235114 (2010).
[41] S. Yao, Z. Yan, and Z. Wang, Topological invariants of Floquet systems: General formulation, special properties, and Floquet topological defects, Phys. Rev. B **96**, 195303 (2017).
[42] M. Tarnowski, F. N. Ünal, N. Fläschner, B. S. Rem, A. Eckardt, K. Sengstock, and C. Weitenberg, Measuring topology from dynamics by obtaining the chern number from a linking number, Nat. Commun. **10**, 1728 (2019).
[43] C. Wang, P. Zhang, X. Chen, J. Yu, and H. Zhai, Scheme to Measure the Topological Number of a Chern Insulator from Quench Dynamics, Phys. Rev. Lett. **118**, 185701 (2017).
[44] C.-K. Chiu, J. C. Teo, A. P. Schnyder, and S. Ryu, Classification of topological quantum matter with symmetries, Rev. Mod. Phys. **88**, 035005 (2016).